Vol. 38 (2007) *ACTA PHYSICA POLONICA B* No 2

ELECTROWEAK SYMMETRY BREAKING WITHOUT HIGGS BOSON*

Efstathios Stefanidis

University College London, Gower Street, London WC1E 6BT, UK

(Received November 15, 2006)

A study is presented of the WW scattering in the absence of a light Higgs Boson. The work is done within the Electroweak Chiral Lagrangian (EWChL) framework, which is extended to high energies using the Padé unitarisation protocol, resulting in potentially new resonances. The generated signal and background processes are simulated using the ATLAS fast simulation package and the discovery potential for multiple scenarios is demonstrated.

PACS numbers: 11.15.Ex, 12.39.q, 12.60.–i, 14.70.Fm

1. Introduction

The Standard Model (SM) of electroweak interactions has been a very successful theory for both theorists and experimentalists, providing an impressive agreement with the precision experimental data [1]. Within the SM, the electroweak symmetry breaking (EWSB) is explained by the Higgs mechanism, which predicts a weakly coupled scalar, the Higgs boson. Over the last years, it is a remarkable achievement how much we have been able to constrain the limits on the Higgs mass (Fig. 1).

However, these limits are model dependent and it is possible that we will see no light scalar particle at all. In that case, a new physics is needed at the TeV scale in order to restore the violated unitarity. The vector boson scattering $V_{\mathrm{L}}V_{\mathrm{L}} \rightarrow V_{\mathrm{L}}V_{\mathrm{L}}$[1] is particularly sensitive to the new physics, since the Goldstone boson responsible for the EWSB becomes the longitudinally polarized component of the gauge bosons $W^{\pm}$ and Z. The EWChL describes the dynamics of the vector boson interactions in a *model independent* way for energies well below the 1 TeV.

---

* Presented at the “Physics at LHC” Conference, Kraków, Poland, July 3–8, 2006.

[1] V denotes both the W and Z bosons.

The Large Hadron Collider (LHC) will be able to study the scattering of gauge bosons in processes like $qqVV \to qqVV$. In this note, the EWChL has been applied in the study of the $W^{\pm}W^{\pm}$ scattering at WW center-of-mass energies of more than 600 GeV.

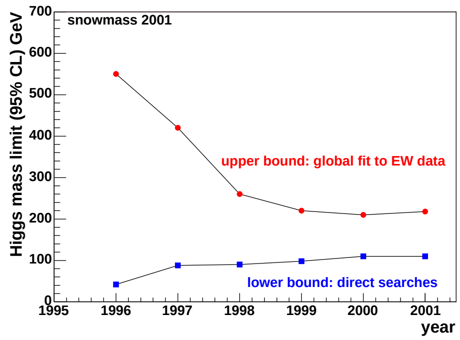

Fig. 1. Upper and lower limit (at 95% C.L) on the Higgs mass. The window of about 500 GeV in 1996 has been reduced to approximately 100 GeV in 2001.

2. The Electroweak Chiral Lagrangian

2.1. Description

The EWChL is based on the Chiral Perturbation Theory [2] and it is a way to describe the low energy effects of different, strongly interacting models of the EWSB sector. It is actually an expansion in derivatives of the Goldstone boson fields and the way for constructing it and its final, complete form are given in [3,4]. For our case, only dimensions up to 4 (or $\hat{s}^2$) are interesting, since these are the terms which describe vector boson scattering. Moreover, there must be a residual SU(2) custodial symmetry, which ensures the equation $M_W^2 = M_Z^2 \cos^2\theta_W$. Taking these constraints into account, the remaining terms of the Lagrangian are:

$$\begin{aligned}\mathcal{L}_{\rm EWChL} = \mathcal{L}^{(2)} + \mathcal{L}^{(4)} &= \frac{u^2}{4}{\rm Tr}\left\{D_\mu U D^\mu U^\dagger\right\} + \alpha_4\left({\rm Tr}\left\{D_\mu U D^\mu U^\dagger\right\}\right)^2 \\ &\quad + \alpha_5\left({\rm Tr}\left\{D_\mu U D^\nu U^\dagger\right\}\right)^2, \end{aligned} \tag{2.1}$$

with

$$U = \exp\left(i\,\frac{\omega^\alpha \tau^\alpha}{u}\right). \tag{2.2}$$

The $\mathrm{SU(2)_L} \bigotimes \mathrm{U(1)}_Y$ covariant derivative of U is defined as:

$$D_\mu U \equiv \partial_\mu U + ig\frac{\tau^\alpha}{2}W_\mu^\alpha U - ig' U\frac{\tau^3}{2}B_\mu\,, \tag{2.3}$$

where τ^{α} ($\alpha = 1, 2, 3$) are the Pauli matrices, ω are the three Goldstone bosons and $u = 246\,\mathrm{GeV}$.

The dependence on the underlying model comes from the dimension-2 terms via the chiral couplings α_4 and α_5: different choices of the value and sign of these parameters would correspond to different underlying (and unknown) theories. Here, it is assumed that their values can vary in the range $[-0.01, 0.01]$ [5].

2.2. Scattering amplitudes

The next step is to calculate the scattering amplitudes. Since we have an $\mathrm{SU}(2)_{\mathrm{L+R}}$ symmetry, we work in the weak isospin space, where the scattering amplitude can be written as:

$$\mathcal{M}(V_{\mathrm{L}}^{a}V_{\mathrm{L}}^{b} \to V_{\mathrm{L}}^{c}V_{\mathrm{L}}^{d}) \equiv A(s,t,u)\delta^{ab}\delta^{cd} + A(t,s,u)\delta^{ac}\delta^{bd} + A(u,t,s)\delta^{ad}\delta^{bc}\,, \quad (2.4)$$

where $V_{\mathrm{L}}^{i} = W_{\mathrm{L}}^{+}, W_{\mathrm{L}}^{-}, Z_{\mathrm{L}}$, and s, t, u are the usual Mandelstam kinematical variables.

The function $A(s,t,u)$ is calculated in [6] up to the order of s^2 and is given by the expression:

$$\begin{aligned} A(s,t,u) \;=\; & \frac{s}{u^2} + \frac{1}{4\pi u^4}\left(2\alpha_4 s^2 + \alpha_5\left(t^2 + u^2\right)\right) \\ & + \frac{1}{16\pi^2 u^4}\left(-\frac{t}{6}(s+2t)\log\left(-\frac{t}{\mu^2}\right)\right) \\ & - \frac{1}{16\pi^2 u^4}\left(\frac{u}{6}(s+2u)\log\left(-\frac{u}{\mu^2}\right) - \frac{s^2}{2}\log\left(-\frac{s}{\mu^2}\right)\right). \end{aligned} \quad (2.5)$$

2.3. Unitarisation and resonance scenarios

The EWChL, as it has been presented, does not respect unitarity as we go to high energies. To restore the unitarity, different unitarisation procedures can be applied. Most commonly, the Padé (or *Inverse Amplitude)* [7] and the N/D [8] protocols have been studied. The unitarised amplitudes result in resonances, the type and the spectrum of which depend on the unitarisation procedure followed. In [9] one can find an investigation and comparison of the two different approaches. For the current analysis, the Padé protocol has been used. The predicted masses and widths are

$$M_{\mathrm{V}}^2 = \frac{u^2}{4(\alpha_4 - 2\alpha_5) + \frac{1}{144\pi^2}}\,, \qquad \Gamma_{\mathrm{V}} = \frac{M_{\mathrm{V}}^3}{96\pi u^2}\,, \quad (2.6)$$

for a vector resonance, whereas for a scalar resonance we get

$$M_{\mathrm{S}}^2 = \frac{12u^2}{16(11\alpha_5 + 7\alpha_4) + \frac{101}{48\pi^2}}\,, \qquad \Gamma_{\mathrm{S}} = \frac{M_{\mathrm{S}}^3}{16\pi u^2}\,. \quad (2.7)$$

The α_4–α_5 parameter space is shown in Fig. 2. A large portion of the parameter space is theoretically excluded [10]. Lines parallel to the dashed or dotted lines correspond to resonances of equal masses and the points which lie at the region from the dotted line and upwards right will correspond to scalar resonances, whereas points inside the region from the dashed line and upwards left will result in vector resonances. Between these two regions, there are two important areas: *(i)* the overlapping area, which will give both a vector and a scalar resonance and *(ii)* a very small region in the parameter space where there will be no resonance at all. In the latest case, the vector boson scattering will result in a *continuum* spectrum. The points A, B, C and D are examples of these scenarios, the characteristics of which are presented in Table I and their differential cross-section in Fig. 2.

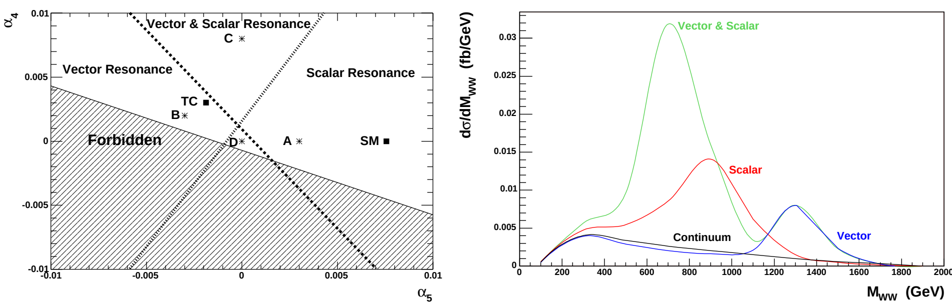

Fig. 2. Left: the α_4–α_5 parameter space as predicted using the Padé protocol. Apart from the points A, B, C and D, examples of a technicolor with $N_{\rm TC}=3$ (point TC) and of a 1 TeV SM Higgs (point SM) are shown [9]. Right: the differential cross-section for the process $W^+W^- \to W^+W^- \to \ell\nu qq$ as a function of the WW mass for the A, B, C and D scenarios.

TABLE I

Values of the α_4 and α_5 parameters and of the masses of the predicted resonances for the A, B, C and D scenarios.

Scenario	α_4	α_5	Resonance Mass (GeV)
Scalar(A)	0.0	0.003	989.8
Vector(B)	0.002	−0.003	1360.3
Scalar + Vector (C)	0.008	0.0	809.6 + 1360.3
Continuum (D)	0.0	0.0	NA

3. Performance

3.1. Monte Carlo event generation and detector simulation

In order to study the scenarios, the PYTHIA [11] Monte Carlo generator was modified to include the EWChL approach and the Padé unitarisation protocol was used. Only $W^{\pm}W^{\pm}$ scattering events were generated and the continuum scenario as signal was used as a case study. The dominant background processes are the $t\bar{t}$ and W+jets production. Both the background and the signal processes are illustrated in Fig. 3. To improve the generation efficiency, the minimum $p_{\rm T}$ of the hard scatter has been set to 300 GeV for the $t\bar{t}$ sample and 250 GeV for the W+jets sample. To simulate the underlying events, the ATLAS Rome-tuning was adopted [12]. The generated events were simulated and reconstructed using the ATLFAST package [13].

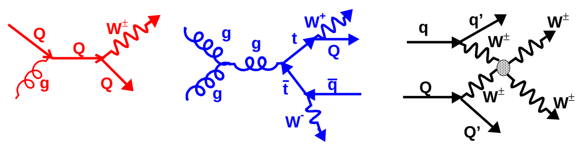

Fig. 3. Diagrams for the W+jets (left), $t\bar{t}$ (center) and WW (right) processes.

3.2. Event reconstruction

We focused on the processes, where one of the bosons decays leptonically ($W \to \ell\nu$, $\ell = e, \mu$) and the other decays hadronically ($W \to qq$).

The leptonically decaying W is reconstructed by the most energetic lepton combined with the missing transverse energy ($E_{\rm T}^{\rm miss}$) of the event. Within the twofold ambiguity, the W with the smallest reconstructed energy was used. For the background and signal processes, the kinematics of the leptonic objects are given in Fig. 4. A cut of 320 GeV is applied on the $p_{\rm T}$ of the leptonic W.

In order to reconstruct the hadronically decaying W, we notice that, since the vector bosons are highly boosted, the final jets will overlap. Keeping that in mind, we reconstruct the hadronic W by the single, most energetic jet in the event. Different clustering algorithms have been studied extensively [14] and for this analysis, the $k_{\perp}$ algorithm [15] with R-parameter $= 0.5$ was found to be the optimum choice. The kinematic distributions are given in Fig. 4. For the hadronic W, we demand $p_{\rm T} > 320$ GeV and 66 GeV $< M_W < 102$ GeV.

An important method, feasible with the $k_{\perp}$, is the subject analysis: using the single jet, the clustering algorithm is re-run over its constituents, trying to find the jet's structure. The scale of the y value at which the jet is resolved into 2 sub-jets is expected to be $\mathcal{O}(M_W^2/p_{\rm T}^2)$, for genuine W. The distribution of the quantity $\log(p_{\rm T} \times \sqrt{y})$ is given in the last histogram of Fig. 4. A cut $1.55 < \log(p_{\rm T} \times \sqrt{y}) < 2.0$ is applied.

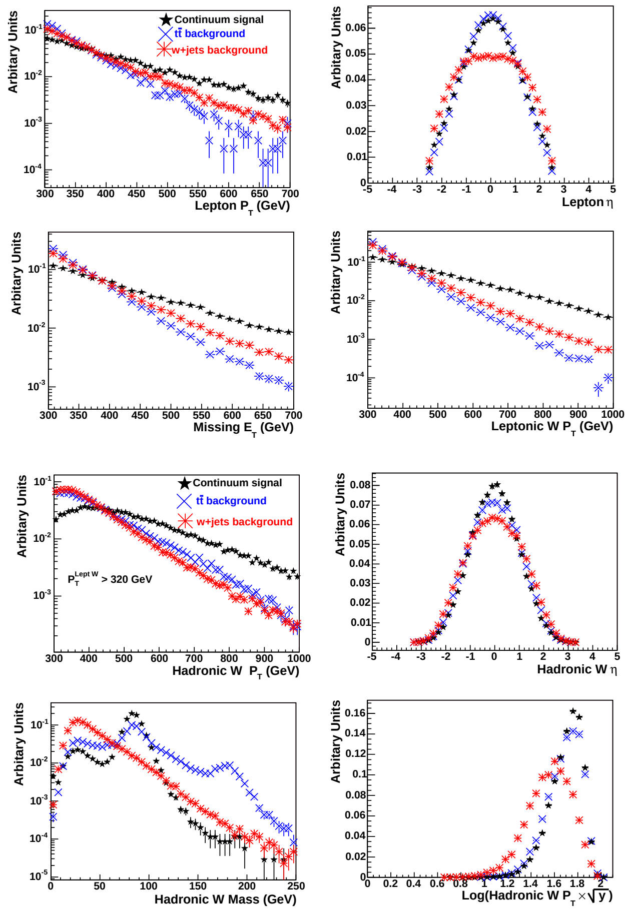

Fig. 4. The kinematic distributions of the reconstructed lepton, E_T^{miss} and leptonic W (four upper figures) and of the hadronic W (four lower figures) for both the signal and background processes. All the histograms are area normalized.

3.3. Background rejection

Finally, we investigate the features, which will further reduce the background as much as possible. Their distributions are given in Fig. 5 and can be summarized as follows:

- **Top Veto**: The jets (excluding the one used of the hadronic W) are combined together with each of the reconstructed vector bosons. For the $t\bar{t}$ sample that would result in reconstructing the top quark. Events with at least one combination in the region $130\,\mathrm{GeV} < \mathrm{M}_{\mathrm{W+jet}} < 240\,\mathrm{GeV}$ are rejected (histograms (a) and (b)).

- **Tag Jets**: In that case we look for the quarks which emitted the two vector bosons. For the signal, these are expected to occupy the very forward regions of the detector. A forward (backward) tag jet is defined as the most energetic jet, which is more forward (backward) of the most forward (backward) W. The pseudorapidity (η) distribution of those jets is presented on the histogram (c). Accepted events are those which have a least one tag jet (both forward and backward) in the region $2.0 < |\eta| < 4.5$.
- **Hard** p_{T}: The combined system of the tag jets and the vector bosons should not have transverse component of their momentum, as it can be seen from Fig. 3. The p_{T} distribution of the system is given on the histogram (d). A cut of 50 GeV is applied.

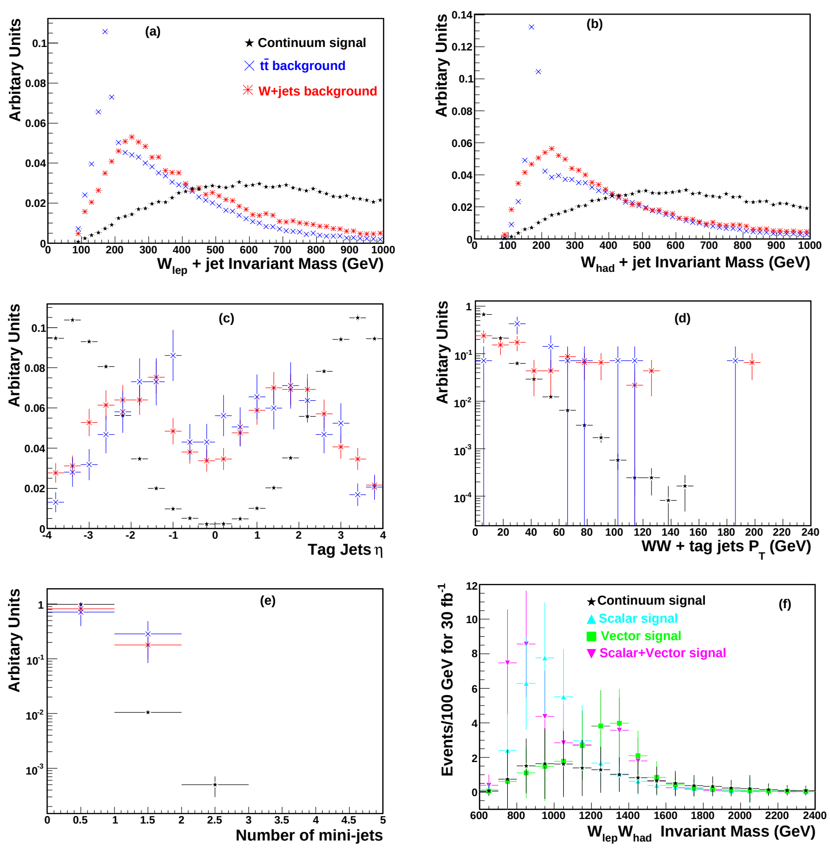

Fig. 5. (a)–(e) The distributions of the hadronic features for both the signal and background samples. (f) The expected number of events for all the scenarios, after background subtraction, as a function of the WW invariant mass.

- **Mini-jet veto**: The mini-jets are defined as all the jets with $p_{\rm T} > 20\,{\rm GeV}$ inside the region $|\eta| < 2.0$. Since there is no color exchange between the quarks which emitted the W bosons and the bosons themselves, we expect no mini-jets. The distribution is given on the histogram (e). Events which have mini-jets are rejected.

4. Results

The effect of each cut on the cross section for both the signal and background samples is presented in Table II. For an integrated luminosity of $30\,{\rm fb}^{-1}$, the significance is also given in the table and the expected number of events for all the scenarios *versus* the invariant mass of the WW system is plotted in the last histogram (f) of Fig. 5. At the end of the analysis, the achieved significance approaches the 5σ, in the case of the continuum scenario, 10.78 for scenario A, 7.16 for scenario B and 13.35 for scenario C.

TABLE II

The effect of the applied cuts (see text) on the cross section for both the signal (continuum scenario) and background samples. The errors are due to statistics only and the significance is given for $L = 30\,{\rm fb}^{-1}$.

Cross section σ (fb)	Signal	$t\bar{t}$	W+jets	Significance
Generated	44	15640	62600	0.86
Cuts:				
$P_{\rm T}$ leptonic W	3.301±0.011	387.481±0.992	2879.670±5.354	0.32
$P_{\rm T}$ hadronic W	2.579±0.009	174.524±0.671	1813.100±4.285	0.32
Mass hadronic W	2.038±0.008	80.739±0.456	208.354±1.472	0.66
Y scale	1.735±0.008	65.839±0.413	114.015±1.090	0.71
Top veto	1.585±0.007	3.308±0.092	52.782±0.742	1.16
$P_{\rm T}, E, \eta$ tag jets	0.449±0.004	0.039±0.010	0.490±0.071	3.38
$P_{\rm T}$ hard scatter	0.439±0.004	0.018±0.007	0.292 ± 0.055	4.32
Number of mini-jets	**0.434±0.004**	**0.013±0.006**	**0.240±0.050**	**4.73**

REFERENCES

[1] `http://lepewwg.web.cern.ch/LEPEWWG`, CERN-EP-200-016, March 2006.

[2] S. Weinberg, *Physica A* **96**, 327 (1979).

[3] A. Dobado, M.J. Herrero, *Phys. Lett.* **B228**, 495 (1989).

[4] A. Dobado, M.J. Herrero, J.R. Pelaez, M.E. Ruiz, *Phys. Rev.* **D62**, 055011 (2000).

[5] A.S. Belyaev *et al.*, *Phys. Rev.* **D59**, 015022 (1999).

[6] M. Golden, T. Han, G. Valencia, `hep-ph/9511206`.

[7] T.N. Truong, *Phys. Rev. Lett.* **61**, 2526 (1988).

[8] G.F. Chew, S. Mandelstam, *Phys. Rev.* **119**, 467 (1960).

[9] J.M. Butterworth, B.E. Cox, J.R. Forshaw, *Phys. Rev.*, **D65**, 096014 (2002).

[10] J.R. Pelaez, *Phys. Rev.* **D55**, 4193 (1997).

[11] T.L. Sjostrand, S. Leif Mrenna, `hep-ph/0108264`.

[12] `https://twiki.cern.ch/twiki/bin/view/Atlas/RomeEvgenWiki`

[13] E. Richter-Was, D.P. Froidevaux, L. Poggioli, ATL-PHYS-98-131.

[14] S. Allwood, Mancherster University, PhD Thesis, 2006.

[15] J.M. Butterworth, J.P. Couchman, B.E. Cox, B.M. Waugh, *Comput. Phys. Commun.* **153**, 85 (2003).